Supporting Information

Distorted Inverse Spinel Nickel Cobaltite Grown on MoS_2 Plate for Significantly Improved Water Splitting Activity

Jiangtian Li,* Deryn Chu,* David R. Baker, Hong Dong, Rongzhong Jiang, and Dat T. Tran

[a] Sensors and Electron Devices Directorate, US Army Research Laboratory, 2800 Powder Mill Road, Adelphi 20783, Maryland

* Corresponding Authors.

Tel: 301-394-0308; Fax: 301-394-0273.

Contents:

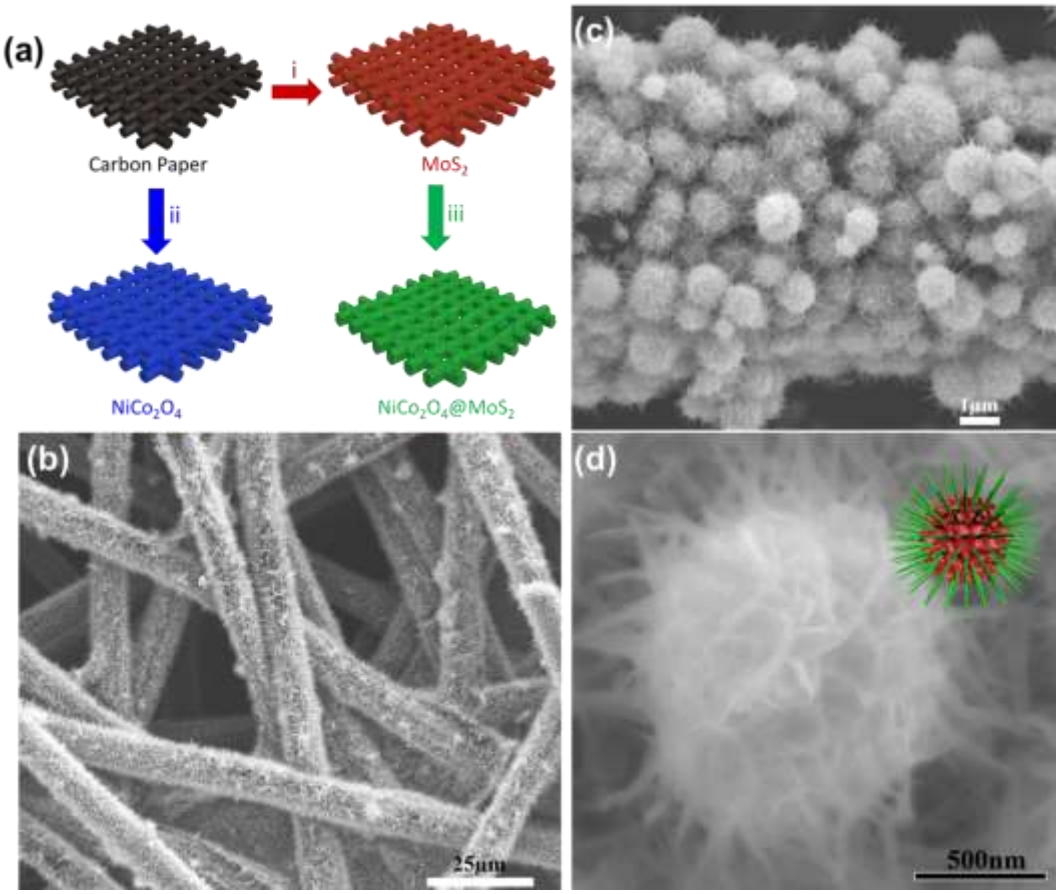

Figure S1. (a) shows the scheme for the preparation of $NiCo_2O_4$, MoS_2 and $NiCo_2O_4$@MoS_2 on carbon fiber with hydrothermal steps. All three steps (i,ii,iii) were carried out with a hydrothermal process. (b) SEM image for $NiCo_2O_4$ nanowire on carbon paper with low magnification. NCO nanowires homogeneously dispersed on carbon fiber. (c, d) SEM images for $NiCo_2O_4$@MoS_2 heterostructures. $NiCo_2O_4$ branches uniformly dispersed on the core-ball, which were turned out to be hollow tube structure in TEM observation.

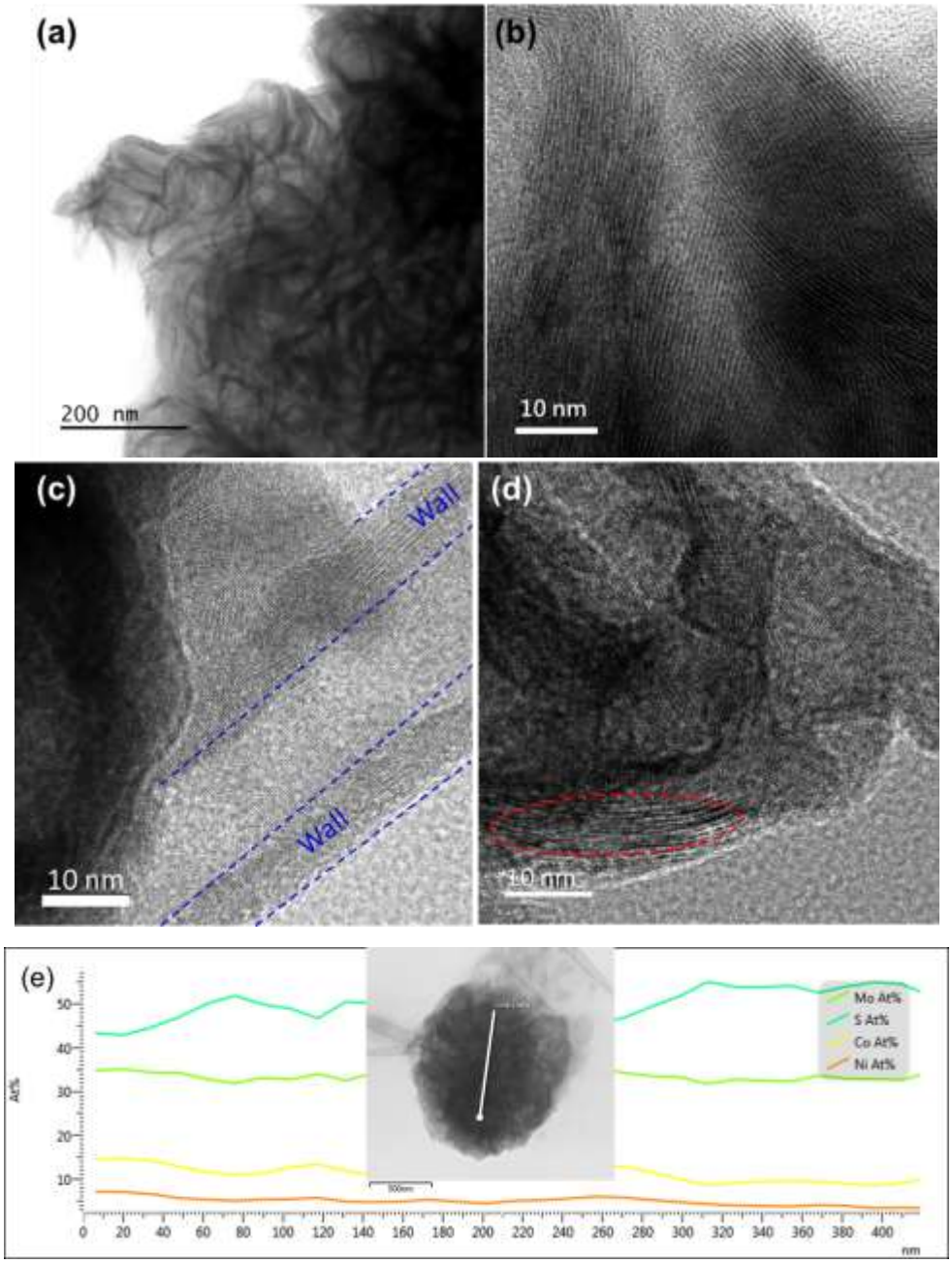

Figure S2. TEM images for MoS_2 balls (*a*, *b*) and $NiCo_2O_4$@MoS_2 heterostructure (*c*, *d*), respectively. Clearly, MoS_2 ball are composed of layered MoS_2 plates (*a*), and the distance between layers is determined to be around 0.79nm (*b*). (*c*) displays the interface where a hollow $NiCo_2O_4$ tube grow from the core-ball. The wall is well crystallized with Ni-Co-O spinel particles. The thickness may vary with each other. (*d*) shows another very faint example of layered MoS_2 plate in heterostructure, where is surrounded with crystallized particles. The distance between layers is measured to be ~0.7nm. (*e*) EDS linear scanning on core-ball area in heterostructure.

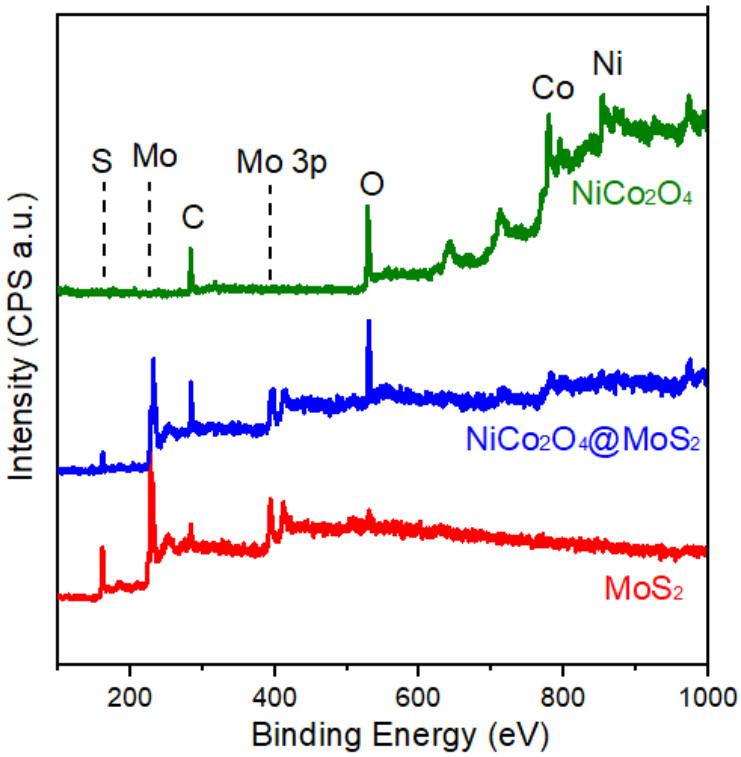

Figure S3. XPS surface survey for $NiCo_2O_4$, MoS_2 and heterostructured $NiCo_2O_4$@MoS_2. Apparently, Mo, S and carbon in MoS_2, Ni, Co, O and C in $NiCo_2O_4$, and all features for both $NiCo_2O_4$ and MoS_2 can be observed in $NiCo_2O_4$@MoS_2 heterostructures.

Table S1. XPS peak position for each element in MoS_2, $NiCo_2O_4$ and $NiCo_2O_4@MoS_2$, respectively.

Samples		$NiCo_2O_4$	MoS_2	$NiCo_2O_4@MoS_2$
Ni 2p3	Ni^{2+}	854.79	-	853.68
	Ni^{3+}	856.77	-	856.97
Co 2p3	Co^{2+}	781.74	-	781.63
	Co^{3+}	779.96	-	779.62
O 2s	O_I	529.72	-	529.35
	O_{II}	531.43	-	531.05
	O_{III}	532.66	-	532.83
S 2p	S 2p3/2	-	161.75	162.59
	S 2p1/2	-	162.95	163.79
Mo 3d	Mo 3d5/2	-	228.99	232.2
	Mo 3d3/2	-	229.73	232.77

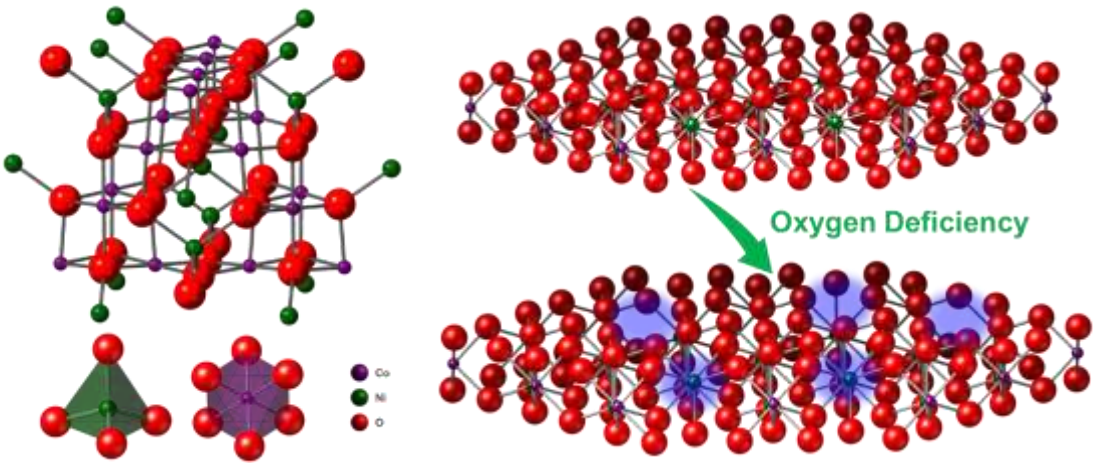

Figure S4. Normal spinel AB_2O_4. (*a*) This crystal structure was produced by replacing Mg and Al with Ni and Co in a standard spinel mine $MgAl_2O_4$. In a standard spinel, A^{2+} coordinates tetrahedrally with four adjacent oxygens, and B^{3+} coordinates octahedrally with six adjacent oxygens. For real $NiCo_2O_4$ crystal, there always co-exist multiple valences for both Ni and Co, that is, Ni^{2+}/Ni^{3+} and Co^{2+}/Co^{3+}. Tetrahedral sites are occupied by Co^{2+} and Co^{3+} ions and octahedral sites are occupied by Ni^{2+}, Ni^{3+} and Co^{3+} ions. This offers multiple active redox couples, and thereby the electrocatalytic activity for chemical reactions. (*b*) shows the structure with metal ions between interstices of two oxygen layers. Such a spinel structure easily generates oxygen deficiency on the surface.

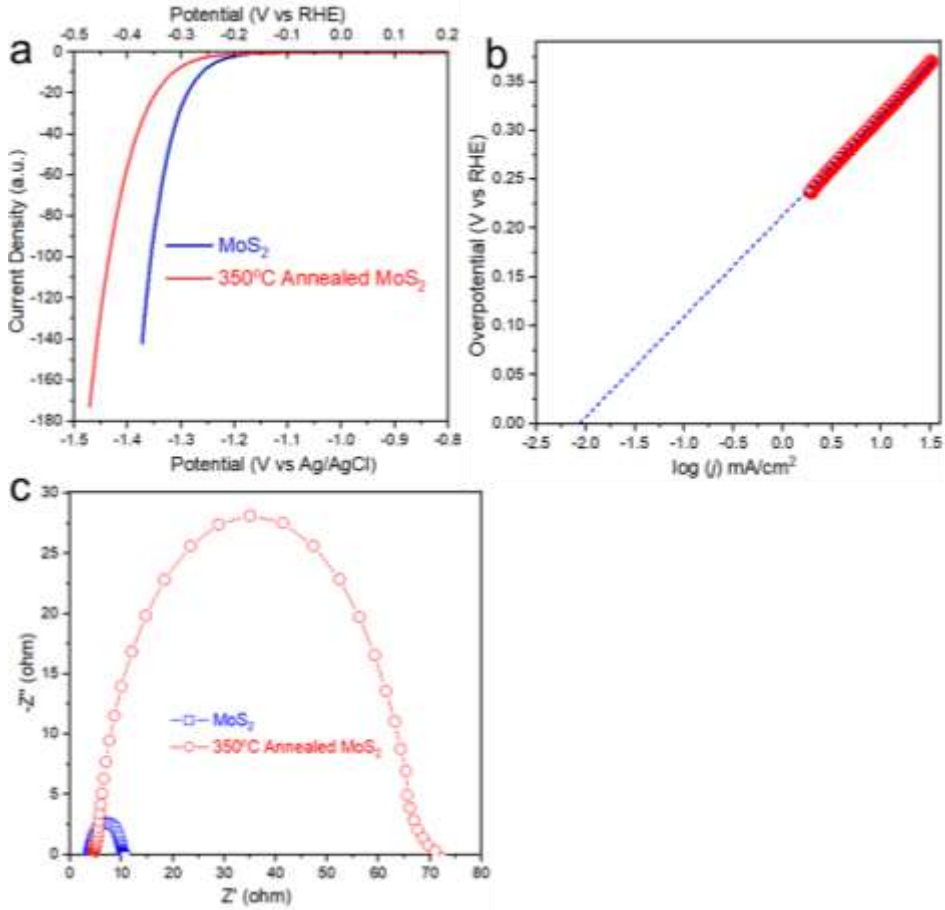

Figure S5. Comparison of HER performance for MoS_2 samples before and after annealing at 350°C under Ar (the same conditions as that for $NiCo_2O_4$@MoS_2 heterostructures). (a) Polarization curves for annealed MoS_2; (b) the corresponding Tafel plots and Exchange current density; (c) Electrochemical Impedance spectra for original and annealed MoS_2/carbon paper sample.

After annealing, HER performance of MoS_2 sample degrades sharply. As shown in Fig S5a, at an overpotential η=300mV, the current density for original MoS_2 sample is 25.9mA/cm^2, while for annealed sample it is 7.7mA/cm^2, only nearly one quarter of the original value. The Tafel slope was calculated to be 106mV/dec, and the corresponding exchange current density j_0 was detected to be 8.7×10^{-3}mA/cm^2, a substantially decrease compared to the original MoS_2 sample (Fig. S5b). Comparison of EIS spectra shows that the charge transfer resistance for HER significantly increased after annealing (Fig. S5b).

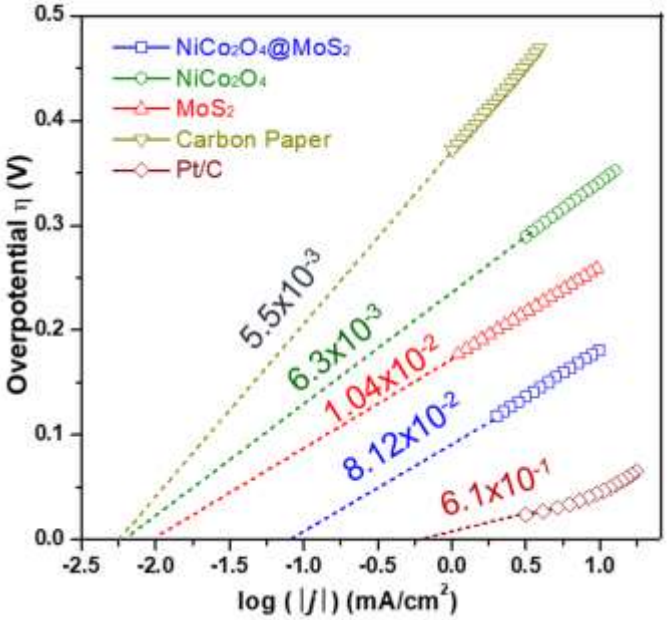

Figure S6. Exchange current density j_0 corresponding to the Tafel plots in Figure 6.

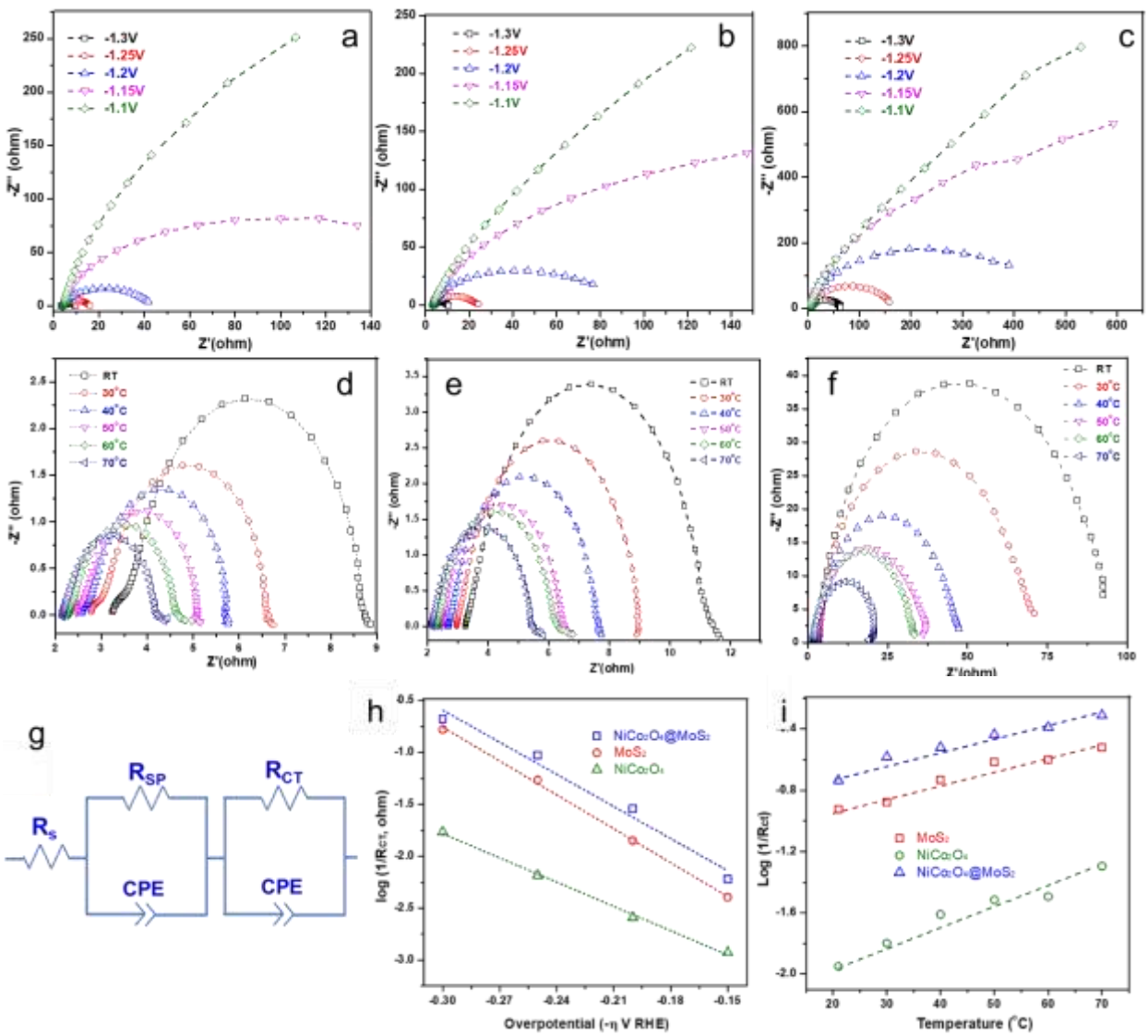

Figure S7. Electrochemical Impedance Spectroscopy (EIS) of potential and temperature dependences of charge transfer behavior R_{ct} as the function of overpotentials (a-c) and temperatures (d-f) for electrode catalysts: (a, d) $NiCo_2O_4$@MoS_2, (b, e) MoS_2 and (c, f) $NiCo_2O_4$, respectively. Temperature dependent EIS spectra were performed with an overpotential η=0.3V vs RHE. (g) the Equivalent circuit used for fitting EIS spectrum in this study. Two-CPE model was to used, one for electrode texture R_{SP}, and the other for charge transfer R_{ct}. (h) Dependence of charge transfer R_{ct} on the overpotential η. (i) the relationship between charge transfer resistance $\log(1/R_{ct})$ with measured temperature.

Regularly, two semicircles were observed on the entire plots, a very small one in the high frequency domain that was almost independent of the potential and temperature, which is attributed to the electrode texture R_{SP}. This feature is clearer for MoS_2 containing catalysts because of the presence of surface pores within the MoS_2 balls. The second semicircle in the middle and low frequency domain that was varied with the potentials, and is attributed to the charge transfer

resistance R_{ct} of HER. The EIS experimental data were therefore approximated with two CPE model equivalent circuit (Fig. g). As shown in Fig. h and Fig. i, both plots of log (1/Rct) versus overpotential (η) and temperature (T) yield a good linear relationship, which means the HER reaction follows the Volmer-Heyrovsky pathway. This is consistent with the conclusion from the Tafel slope prediction.

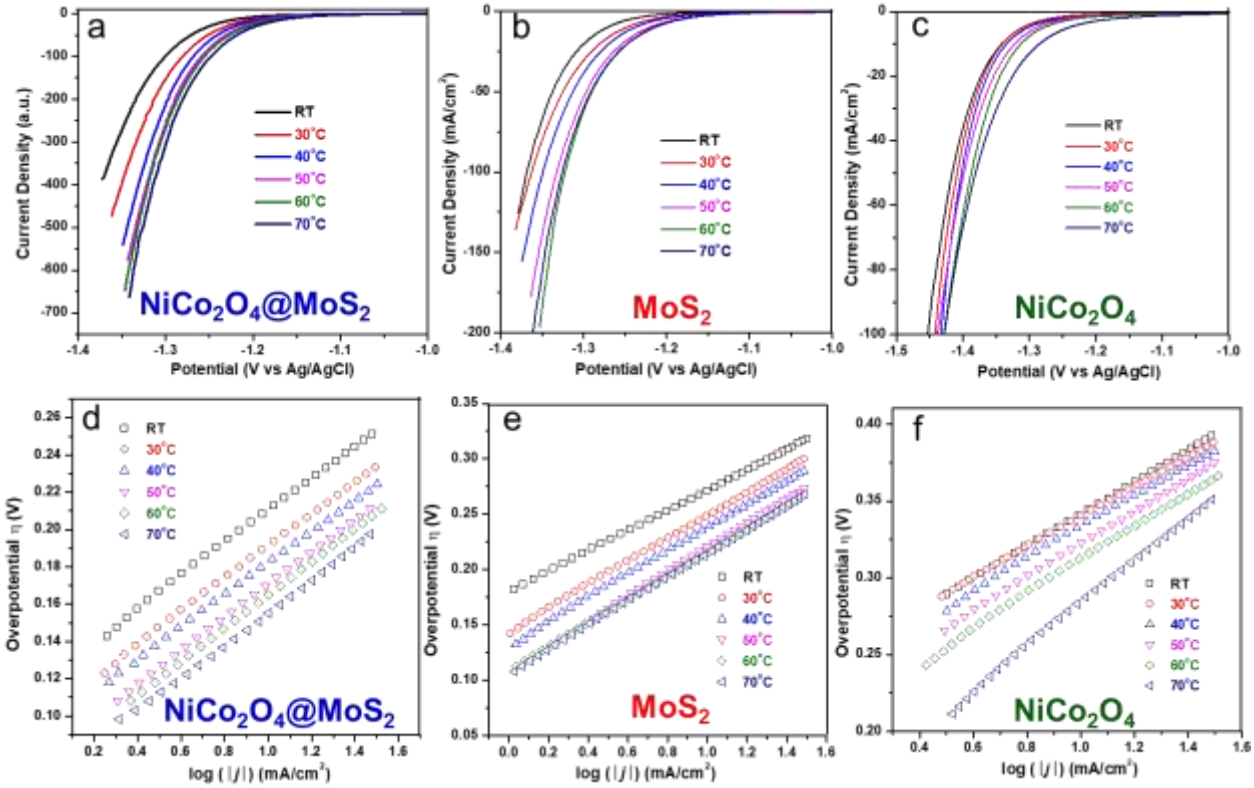

Figure S8. Polarization curves as the function of temperatures and the corresponding temperature dependent Tafel plots for electrode catalysts, (a, d) $NiCo_2O_4$@MoS_2, (b, e) MoS_2 and (c, f) $NiCo_2O_4$, respectively.

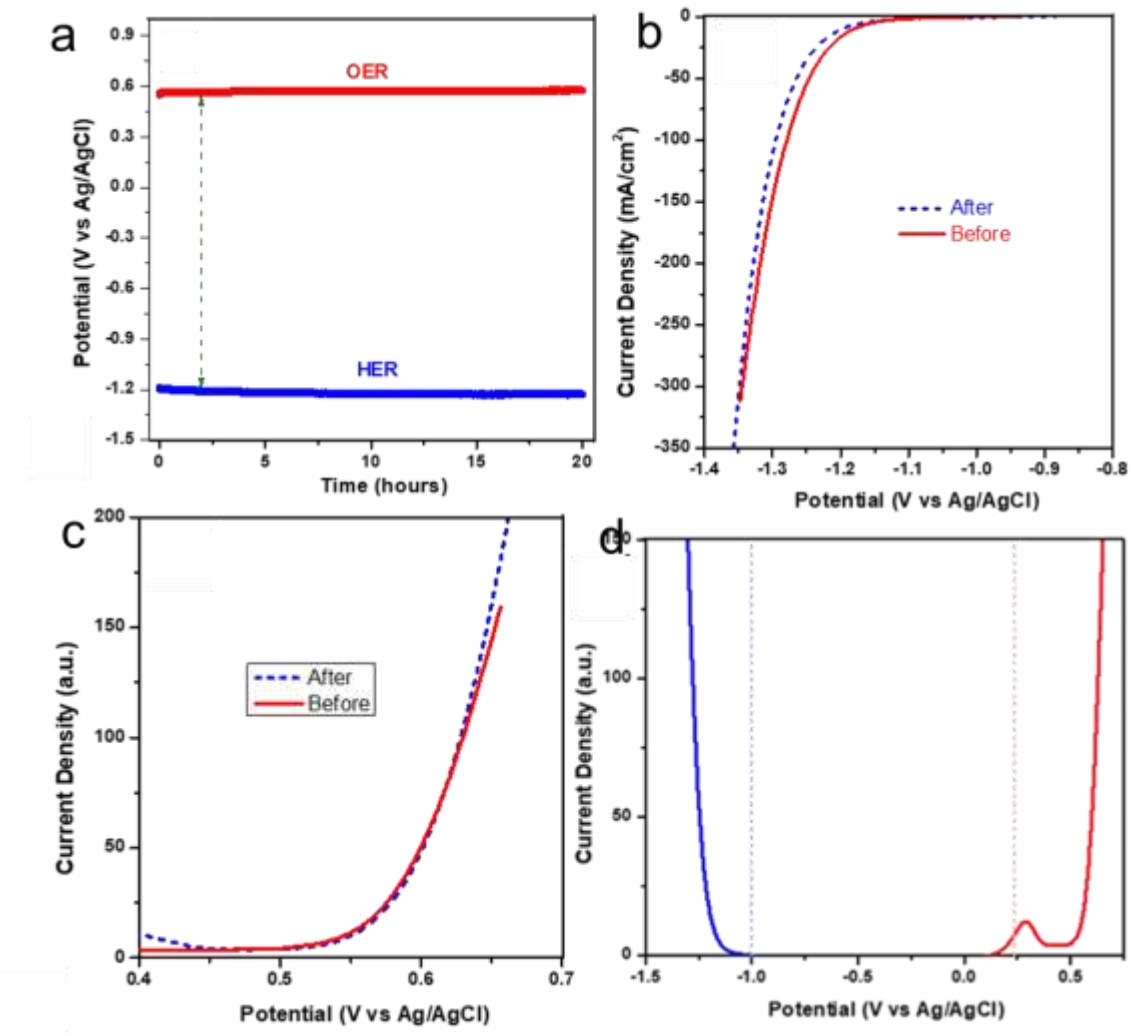

Figure S9. OER and HER Stability of heterostructured $NiCo_2O_4$@MoS_2 catalyst. (a) Stability test of $NiCo_2O_4$@MoS_2 catalyst for both HER and OER for 20 hours with constant current density of 10mA/cm^2. (*b*, *c*) polarization curves before and after the 20 hours HER and OER stability testing. (d) Coupled HER and OER polarization curves giving the overpotential for overall water splitting. The inset compares the overpotential required for overall water splitting reaching a current density of 10mA/cm^2

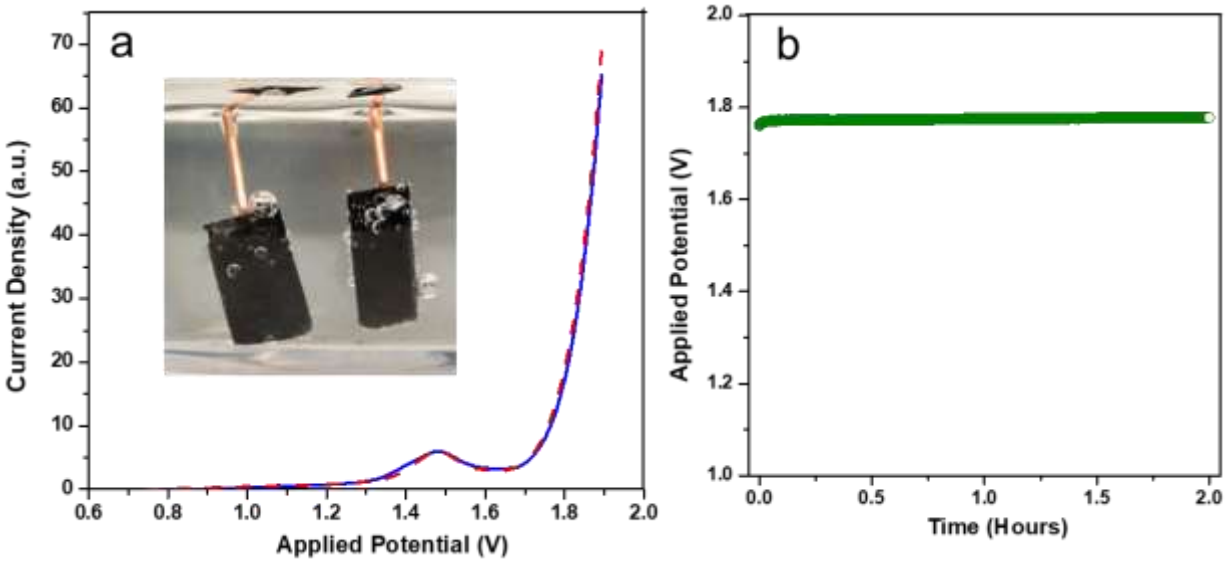

Figure S10. Overall water splitting using heterostructured $NiCo_2O_4@MoS_2$ catalyst as both cathode and anode. (*a*) polarization curves in a two-electrode configuration cell. (*b*) stability curves show the potential variation with a constant current density of 10mA/cm^2. The Inset in *a* shows the two $NiCo_2O_4@MoS_2$ electrodes with bubbles.